Heliyon 10 (2024) e27458

Contents lists available at ScienceDirect

Heliyon

journal homepage: www.cell.com/heliyon

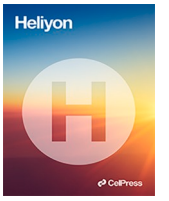

Research article

Protective effect of *Inonotus obliquus* polysaccharide on MGO-induced nonenzymatic glycation fibroblasts

Chunyu Chen [a,b], Xiaoxing Liu [a,b], Yingying Lin [a,b], Li Li [a,b], Miaomiao Guo [a,b], Fan Yi [a,b,*]

[a] *Beijing Key Laboratory of Plant Resources Research and Development, Beijing Technology and Business University, No. 11, Fucheng Road, Haidian District, Beijing, 100048, PR China*

[b] *Key Laboratory of Cosmetic, China National Light Industry, Beijing Technology and Business University. No. 11, Fucheng Road, Haidian District, Beijing, 100048, PR China*

ARTICLE INFO

Keywords:
Nonenzymatic glycation
AGEs
CML
Inonotus obliquus polysaccharide
Skin behavior disorder

ABSTRACT

Background: The nonenzymatic glycation of fibroblasts causes functional downregulation and behavioral disorders in the skin.

Methods: To investigate the effect of *Inonotus obliquus* on the nonenzymatic glycation of skin, we examined the inhibition of advanced glycation end products (AGEs) using four extraction methods: n-butanol, ethyl acetate, n-hexane and aqueous alcohol precipitation. The physical properties and chemical structure of the most effective, purified, crude *I. obliquus* polysaccharide (IOP) were examined. The effects of IOP on carboxymethyl lysine (CML) accumulation, inflammatory factor release, reactive oxygen species (ROS) production, key extracellular matrix (ECM) protein (MMP 1, 2 and 9; FN-1, LM-5 and COL-1) mRNA expression, and cell survival, migration and adhesion were also examined via cellular assays.

Results: IOP is a polysaccharide with a molecular weight (Mw) of 2.396×10^4 (±6.626%) that is composed mainly of glucose, galactose, xylose, mannose and arabinose (29.094:21.705:14.857:9.375:7.709). In addition, a cellular antiglycation assay showed that IOP, which can promote ECM formation by inhibiting the accumulation of CML, inhibiting the release of inflammatory factors (IL-1β, IL-6, and TNF-α), inhibiting the production of reactive oxygen species (ROS), inhibiting the expression of matrix metalloproteinases (MMP-1\-2\-9), promoting the synthesis of ECMs (COL1, FN1, and LM5), and improving cellular dysfunction, had strong antiglycation activity at concentrations in the range of 6–24 μg/mL.

Conclusion: IOP effectively reduced the levels of inflammatory factors and reactive oxygen species produced by AGEs, further preventing the impairment of cell behavior (decreased migration and reduced cell adhesion) and preventing the downregulation of the expression of key extracellular matrix proteins induced by AGEs. The results indicate the potential application of IOP as an AGE inhibitor in skin care.

* Corresponding author. Beijing Key Laboratory of Plant Resources Research and Development, Beijing Technology and Business University, No. 11, Fucheng Road, Haidian District, Beijing 100048, PR China.
E-mail address: fantasyee@btbu.edu.cn (F. Yi).

https://doi.org/10.1016/j.heliyon.2024.e27458
Received 27 September 2023; Received in revised form 28 February 2024; Accepted 29 February 2024
Available online 8 March 2024

1. Introduction

The worldwide epidemic of diabetes and its associated complications are serious public health concerns. Epidemiological surveys have shown that 463 million people had diabetes in 2019, and 700 million adults worldwide are expected to be diagnosed by 2045 [1]. Among these, 30%–70% of diabetic patients may develop skin lesions [2], such as skin infections, chronic ulcers, and slow healing wounds. These diabetic skin complications severely affect the quality of life of patients and are closely associated with the accumulation of large amounts of advanced glycation end products (AGEs) in the body [3].

AGEs are a class of glycosylation products formed by the reaction between glucose or another reducing sugar and the free amino acids in proteins, nucleic acids, or lipids. These brown, fluorescent, crosslinked structures, which were first proposed by the French chemist Maillard in 1912, can form in living organisms during the late stages of the Maillard reaction [4]. Many studies have found that AGE accumulation in the skin is the underlying cause of slow diabetic wound healing [5]. On the one hand, AGEs disrupt the balance between the synthesis and degradation of the extracellular matrix (ECM) by upregulating the expression of matrix metalloproteinases (MMPs), such as MMP-9 and MMP-2, leading to dysfunctional fibroblast behavior (proliferation, migration, and adhesion) and impaired ECM remodeling; thus, AGEs interfere with the deposition of the ECM during wound healing [6,7]. On the other hand, AGEs have been shown to interfere with skin healing mechanisms by inducing reactive oxygen species (ROS) production and oxidative stress and further amplifying the proinflammatory response; as a result, diabetic patients experience skin ulcers that often deteriorate into nonhealing wounds [8]. Together, previous studies have shown that the AGE-induced behavioral dysfunction of fibroblasts, oxidative stress, and overexpression of inflammatory factors lead to cellular damage; thus, the dynamic homeostasis of the skin cannot be maintained, and the healing mechanisms in the skin are ultimately disrupted [9,10]. Therefore, the use of AGE inhibitors is a key method for improving skin complications in chronic metabolic diseases, and the development of AGE inhibitors to protect the normal functions of skin cells is an important therapeutic direction for alleviating skin lesions and improving the skin condition of patients.

Researchers worldwide are investigating the use of AGE inhibitors through different methods to treat disease complications [11,12]. AGE inhibitors can be divided into two main categories: synthetic and natural. Synthetic inhibitors, such as aminoguanidine and metformin, have been shown to inhibit AGEs, but these substances still have many side effects and safety concerns because they cause reduced liver function, gastrointestinal disorders, headaches, FLUS and lupus-like symptoms [13]. Aminoguanidine is often used as a positive control in antiglycation assays due to its better antiglycation effect [14,15]. However, there is a lack of test data on aminoguanidine in human skin. Moreover, metformin, a first-line drug for the treatment of type 2 diabetes mellitus, is used in the dermal field to combat skin diseases such as acne [16]. Inhibitors of AGEs in the skin care field are insufficient. Natural bioactive substances that are derived from food and inhibit AGEs have attracted the interest of researchers worldwide, and their few side effects, low toxicity, and ease of production through technological advances make these materials the most promising research direction and trend for AGE inhibitors [17].

As early as the 16th century, *I. obliquus* was widely used in Russia and other Eastern European countries as a folk medicine due to its high safety and low toxicity. *I. obliquus* can grow in hostile environments characterized by seasonal temperature fluctuations, a cold climate, UV radiation and susceptibility to bacterial and viral interference. Therefore, *I. obliquus* produces numerous active substances that form a complex defense system against external stimuli [18]. Many studies have shown that bacteria contain polyphenols, polysaccharides, triterpenoids, melanin and other substances with antiviral, antioxidant, and anti-inflammatory properties and that these substances regulate the blood sugar levels, blood lipids and immune functions [18,19]. It has been shown that *I. obliquus* can alleviate diabetes and kidney damage by regulating oxidative stress and inflammatory factors and has potential as an AGE inhibitor [20,21]. However, the main active component of *I. obliquus* that inhibits AGEs has not yet been identified, and its ability to protect the skin of patients with diabetes (the population) and the possible underlying mechanisms have not been systematically studied.

Therefore, in this study, *I. obliquus* extract was further extracted with different polar solvents. After assessing the in vitro antiglycation activity of each extracted fraction, *I. obliquus* polysaccharide (IOP) was identified as the main active fraction that exerts antiglycation effects, and its potential inhibitory mechanism was dissected. The structure and function of IOP are closely related, and the conformational relationship and activity mechanism of IOP were studied through accurate analyses of the polysaccharide structure. The physical properties and chemical structures of the purified polysaccharide fractions were characterized by Fourier transform infrared (FT-IR) spectroscopy, gel permeation chromatography (GPC), high-performance liquid chromatography (HPLC), and atomic

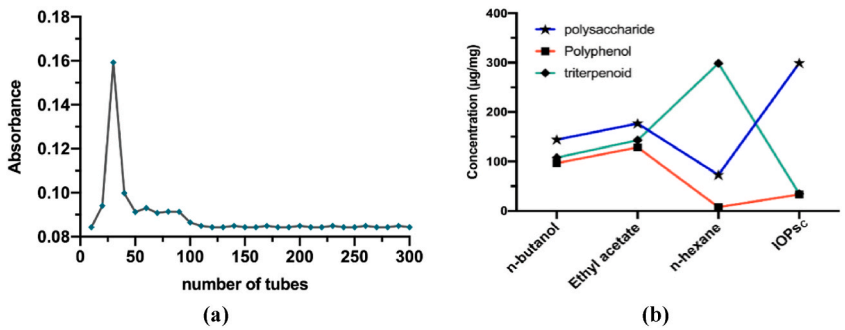

Fig. 1. AB-8 elution profiles of IOP (a) and polysaccharide, polyphenol and triterpene contents in the different extracts (b).

force microscopy (AFM), and the ameliorative effects of these fractions on methylglyoxal (MGO)-induced behavioral dysfunction, oxidative stress and inflammation in human skin fibroblasts based on AGE inhibition were investigated. The results provide a theoretical basis for using IOP to alleviate skin lesions in diabetic patients and improve the condition of the skin in the population.

2. Results

2.1. Polysaccharide, polyphenol and triterpenoid contents

The process used for IOP isolation and purification is shown in Fig. 1a. We examined the contents of total polysaccharides, total polyphenols and total triterpenes in the four extract fractions, as shown in Fig. 1b. Among the four fractions (n-butanol, ethyl acetate, n-hexane and aqueous alcohol precipitation (crude polysaccharide, IOPsc)), the n-hexane fraction had the highest percentage of total triterpenes, and the IOPsc fraction had the highest percentage of polysaccharides; both of these were higher than 300 μg/mg, but the other two components were present at extremely low levels. In addition to the total polysaccharide content, the total polyphenol and total triterpene contents in both the n-butanol and ethyl acetate fractions were low, ranging from 100 to 180 μg/mg.

2.2. Nonenzymatic glycation inhibition capacity

As shown in Fig. 2a, IOPsc obtained from aqueous alcohol precipitation had the highest rate of AGE inhibition, reaching 88% inhibition at a concentration of 125 μg/mL. Furthermore, to investigate the blocking mechanism of IOPsc during AGE formation, we measured the content of glycated serum proteins and carbonylation in the incubation system after 3 and 4 days of incubation, respectively, as shown in Fig. 2b. A concentration of 125 μg/mL resulted in 42% and 58% inhibition of the expression of glycated serum proteins and carbonylation, respectively. The inhibitory effects of the highest concentration (1000 μg/mL IOP) on glycated serum proteins and carbonation were 70% and 84%, respectively, which showed that IOPsc played a role in blocking the production of both glycated serum proteins and carbonation.

2.3. Structural characterization and analysis of the characteristics of IOP

Fig. 3a shows the full-wavelength scan of IOP performed with a UV spectrophotometer. As shown in Fig. 1, IOP exhibited no unique UV absorption peaks at 260–280 nm. This finding indicates that IOP does not contain impurities such as proteins or nucleic acids. The IR spectrum of IOP is shown in Fig. 3b. The absorption peak at 3435 cm^{-1} indicates the presence of an O–H stretching vibration, which is a characteristic absorption peak of sugars, suggesting that IOP contains intermolecular hydrogen bonds. In contrast, the peak at 2935 cm^{-1} is attributed to C–H stretching vibrations, which is typical of polysaccharides. The characteristic absorption peak at 1610 cm^{-1} is caused by the binding of water to a sugar compound. The absorption peak at 1400 cm^{-1} is attributed to the stretching vibration of C═C and the deformation vibration of C–H. The peak at 823 cm^{-1} is characteristic of α-glycosidic bonds. The abovementioned results indicate that birch fucose polysaccharide (IOP) has absorption peaks characteristic of typical polysaccharides [22]. As shown in Fig. 3c and d, IOP is composed of polysaccharides with an average molecular weight of 2.396×10^4 (±6.626%) and contains mainly glucose, galactose, xylose, mannose, and arabinose (29.049:21.705:14.857:9.375:7.709).

The surface morphology and ultrastructure of IOP were investigated via AFM. As shown in Fig. 3e, IOP exhibited irregular polymer particles in water, probably due to the aggregated crosslinking of the sugar chains. The thickness of the IOP chains was 0.6–3.2 nm, which is greater than that of single-chain polysaccharide molecules (0.1–1.0), indicating that the intra- and intermolecular van der Waals forces and hydrogen bonds in IOP became intertwined to form polymers [23]. The average roughness of IOP was 0.4443.

Thermal stability is an important characteristic of materials for biological applications. Additionally, studying the changes in polysaccharide properties, such as dehydration and dissociation, during heating provides a theoretical basis to determine the optimal thermal sterilization temperature for ensuring the stability and biological activity of polysaccharide samples in the food industry [24].

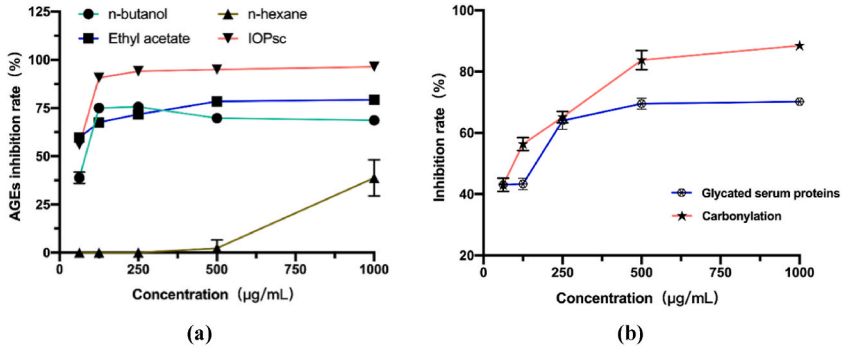

Fig. 2. Inhibition of AGE production by the different extracts (a) and inhibition of the main compounds produced during AGE production by IOP (b).

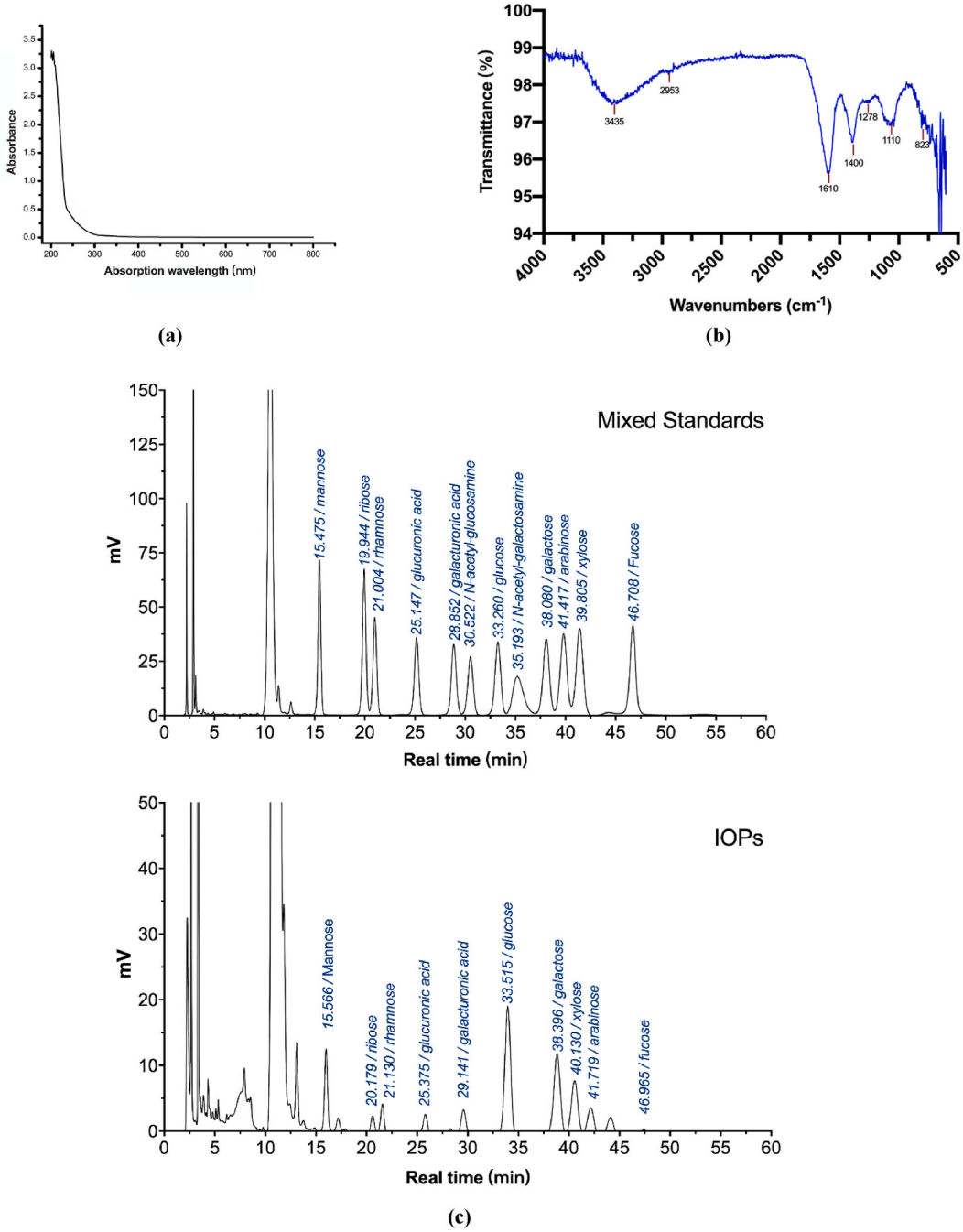

Fig. 3. Structural characterization and physical properties of IOP. UV–Vis spectral analysis of IOP (a), FT-IR-based structural characterization of IOP (b), HPLC-based monosaccharide composition analysis of IOP (c), GPC-based molecular weight analysis of IOP (d), AFM analysis of IOP (e), and thermogravimetric analysis of IOP (f).

As shown in Fig. 3f, the TG curve of IOP shows that the thermal degradation process can be divided into two stages. The first mass loss occurred between 30 °C and 200 °C and was probably due to loss of bound and free water from the polysaccharide polymer. The second degradation stage occurred between 200 °C and 600 °C and had a mass loss of 44%, which may be due to the chemical bonds of polysaccharide molecules breaking down at high temperature. These results indicate that IOP exhibits good thermal stability and can be used as an additive in food systems.

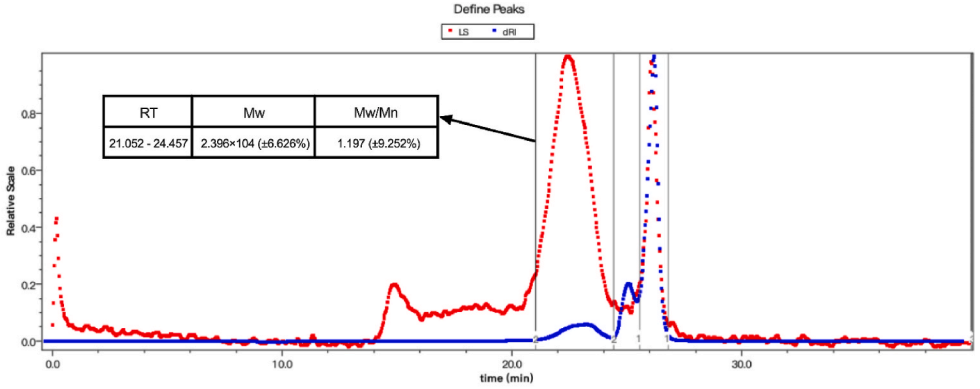

(d)

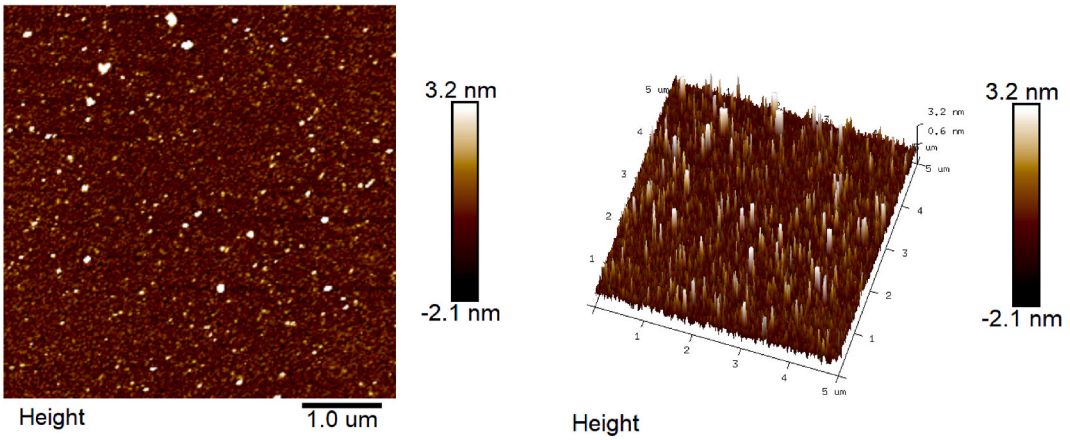

(e)

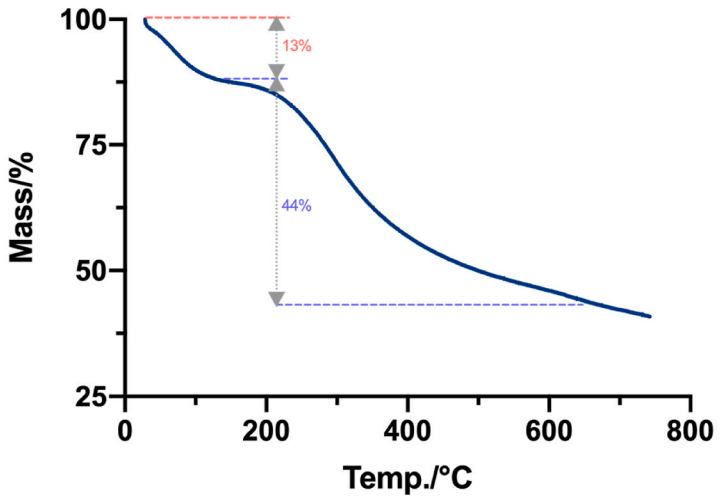

(f)

Fig. 3. (*continued*).

2.4. Effects of IOP on CML and inflammatory factor production induced by MGOs

We then examined whether the treatment of human skin cells with IOPsc (which yielded the best inhibition of AGEs in vitro) reduced the accumulation of AGEs and further blocked AGE-induced cellular inflammatory factor secretion. We stimulated skin fibroblasts with 4 mM MGO to promote nonenzymatic glycation reactions and incubated the skin fibroblasts with 6, 12 and 24 μg/mL IOP to determine the concentrations of CML, one AGE, and inflammatory factors (IL-1β, IL-6 and TNF-α, respectively). As shown in Fig. 4a, IOP significantly reduced the accumulation of CML stimulated by MGO from 95 pg/μg protein to approximately 45 pg/μg protein (24 μg/mL IOP), which is comparable to that found in the blank cells. Furthermore, as shown in Fig. 4b–d, the reduction in CML accumulation similarly slowed the production of inflammatory factors that resulted from an increase in CML. The gradual decreases in the concentrations of inflammatory factors in the range of 6–24 μg/mL were similar to those observed in the blank group.

2.5. Relative mRNA expression of key proteins

As shown in Fig. 5a–c, MMP-1, MMP-2 and MMP-9 were differentially downregulated by 6–24 μg/mL IOP, especially 12 and 24 μg/mL IOP (***, $p < 0.001$); moreover, the relative mRNA expression of MMPs was slightly lower than 1. Accordingly, the relative mRNA expression levels of type I collagen, fibronectin and laminin, which are important components of the ECM, were significantly upregulated after incubation with IOP, especially at 24 μg/mL. As shown in Fig. 5d–f, upregulated expression of type I procollagen (from 0.59 to 0.88), FN-1 (from 0.63 to 1.12), and laminin-5 (from 0.5 to 2.15) was observed under MGO stimulation. Based on the abovementioned experiments, we selected 24 μg/mL IOP for subsequent experiments.

2.6. IOP ameliorated MGO-induced oxidative stress in fibroblasts

When excessive ROS disrupt homeostasis within the antioxidant system, the resulting indiscriminate oxidation of proteins, lipids and nucleic acids can lead to the development of oxidative damage, inflammatory responses, functional cellular disorders and even apoptosis. To investigate whether IOP can effectively reduce the intracellular ROS content under MGO stimulation, we stimulated CCC-ESF-1 cells with 4 mM MGO. As shown in Fig. 6, the ROS level in the stimulated CCC-ESF-1 cells was significantly increased. The fluorescence threshold increased from 6700 to 9850 in the blank group (***, $p < 0.001$), whereas cells treated with 24 μg/mL IOP

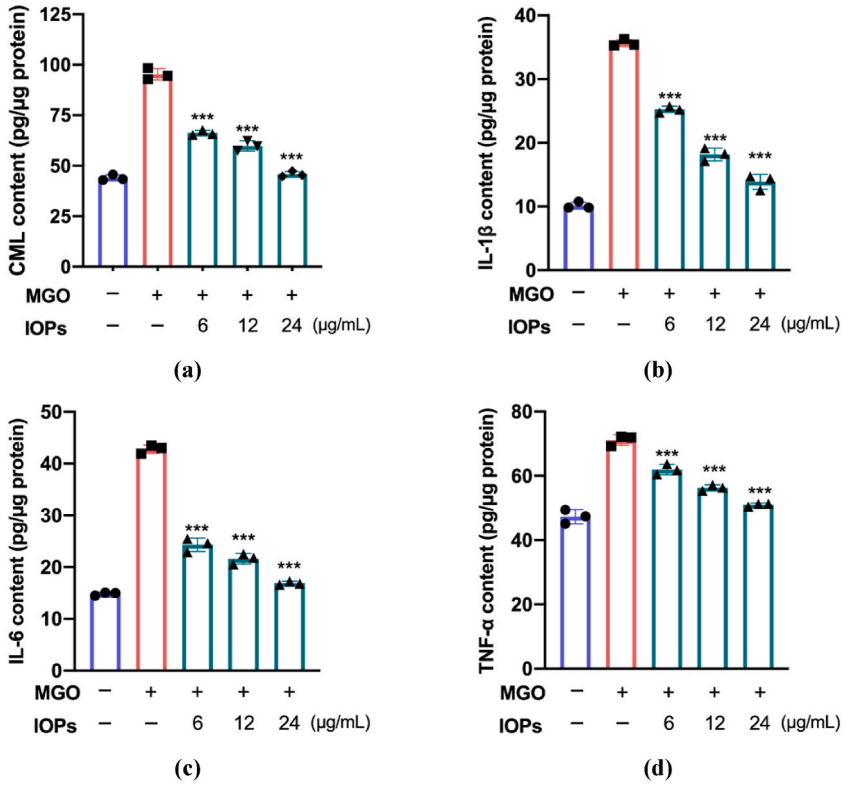

Fig. 4. The cellular CML expression in fibroblasts treated with different concentrations of IOP after MGO-induced nonenzymatic glycosylation was determined by ELISA; the data are expressed as the means ± standard deviations (n = 3) (a). The expression of IL-1β, IL-6, and TNF-α in fibroblasts treated with different concentrations of IOPs after MGO-induced nonenzymatic glycosylation was determined via ELISA, and the data are presented as the means ± standard deviations (n = 3) (b, c, d). Statistical analyses were performed by one-way ANOVA to identify significant differences.

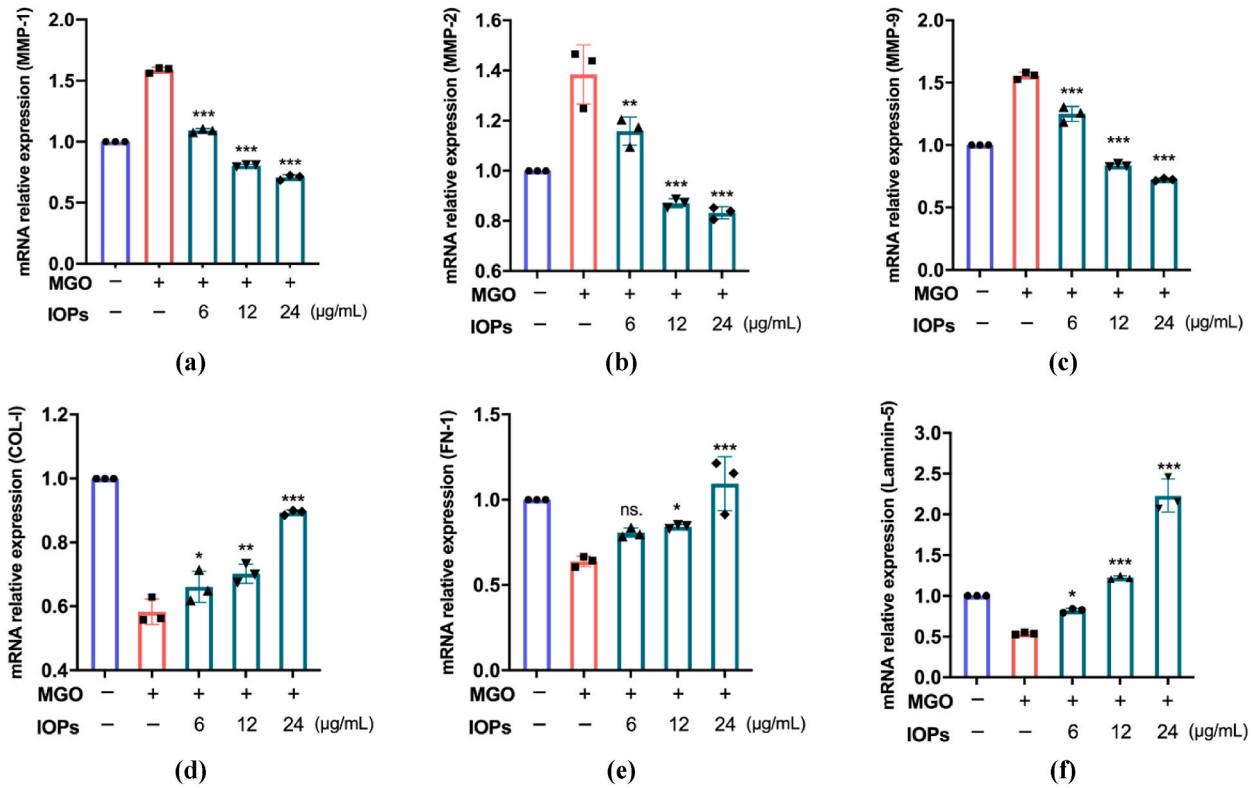

Fig. 5. The effects of different concentrations of IOP on intracellular matrix metalloproteinase family (MMP) gene transcription (a–c), COL-I gene transcription (d), FN-1 gene transcription (e), and laminin-5 gene transcription (f) in fibroblasts treated with different concentrations of IOP after MGO-induced nonenzymatic glycosylation were determined by qRT−PCR. The data are expressed as the means ± standard deviations (n = 3). Statistical analyses were performed by one-way ANOVA to identify significant differences.

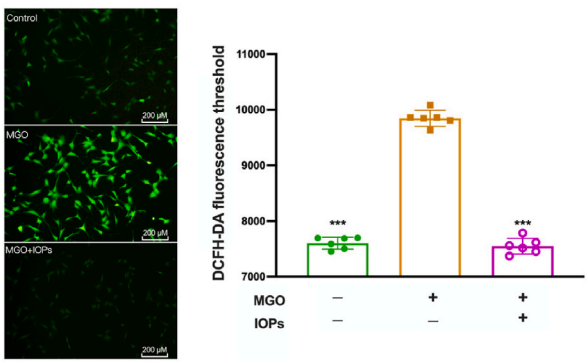

Fig. 6. The intracellular reactive oxygen species (ROS) concentration in fibroblasts treated with IOP after MGO-induced nonenzymatic glycosylation was determined via immunofluorescence. The data are expressed as the means ± standard deviations (n = 6). Statistical analyses were performed by one-way ANOVA to identify significant differences.

under 4 mM MGO stimulation did not show an increase in ROS, and the fluorescence threshold remained similar to that of the blank group at 6500.

2.7. Protective effect of IOP on cells induced by MGO

To investigate whether IOP can prevent or treat cell behavior disorders caused by MGO stimulation, we analyzed the survival, migration rate and adhesion of cells. First, we stimulate CCC-ESF-1 cells with different concentrations of MGO (2–8 mM) and established a control group (24 μg/mL IOP) for each concentration. As shown in Fig. 7a, under different concentrations of MGO

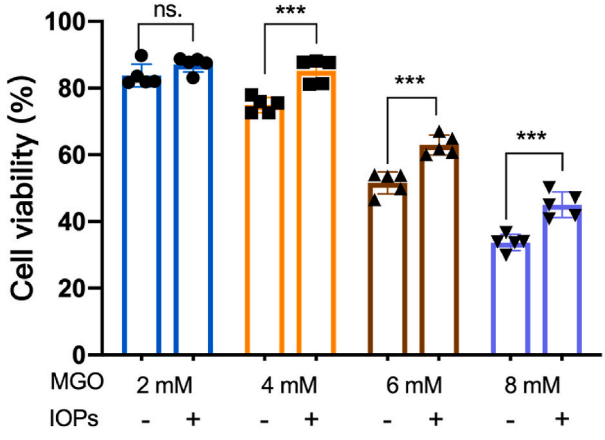

(a)

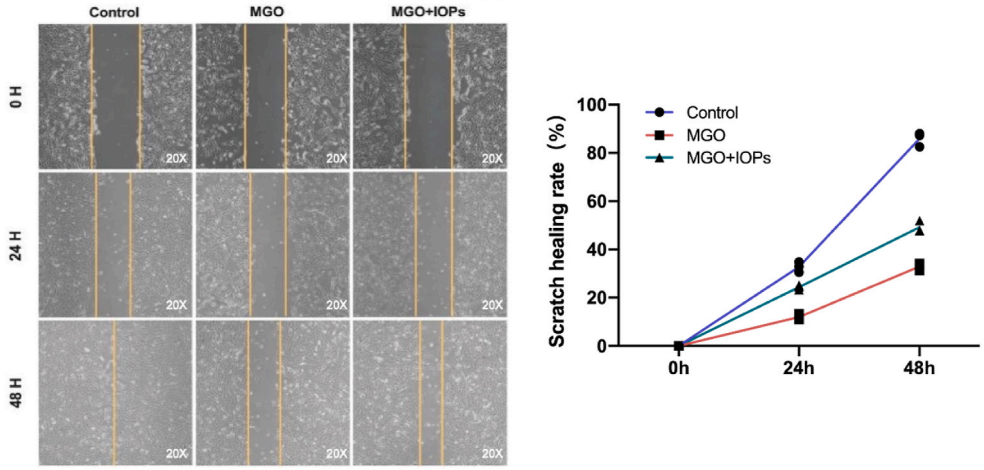

(b)

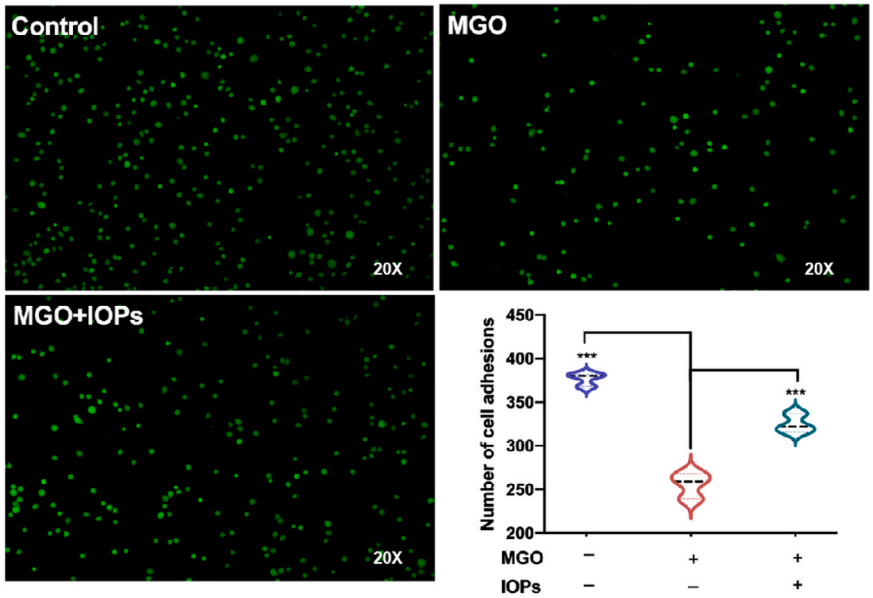

(c)

(caption on next page)

Fig. 7. Fibroblasts were subjected to MGO-induced nonenzymatic glycosylation followed by IOP treatment. (a) The effect of IOP on the proliferation of CCC-ESF-1 cells stimulated with different concentrations of MGO was determined by a CCK8 assay (the data are presented as the mean ± standard deviation (n = 5)). Statistical analyses were performed by one-way ANOVA to identify significant differences. (b) The effect of IOP on MGO-stimulated cell migration was determined by a scratch assay (the data are presents as the means ± standard deviations (n = 3)). (c) The effect of IOP on MGO-stimulated cell adhesion was determined by fluorescence assay (the data are presented as the means ± standard deviations (n = 5)). Statistical analyses were performed by one-way ANOVA to identify significant differences.

stimulation, 24 μg/mL IOPs can improve cell survival. As shown in Fig. 7b, we observed the migration of the cells at 0 h, 24 h and 48 h and found that migration was significantly decreased in the presence of MGO; specifically, the migration rate decreased by 23% and 53% at the 24 h and 48 h time points, respectively. In contrast, the cell migration rate of the IOP treatment group was increased by 12% and 14% at the 24 h and 48 h time points compared with that of the model group, respectively. As shown in Fig. 7c, under the same conditions, MGO caused an extremely significant decrease in cell adhesion from 383 cells/region to 264 cells/region (***, $p < 0.001$), whereas incubation with IOP significantly increased cell adhesion, which remained at 332 cells/region.

3. Discussion

In the present study, the polysaccharide fraction (IOP) was isolated and purified from *I. obliquus* extracts, and the protective effect of IOP on dermal fibroblasts in a glycosylation environment induced by stimulation with MGO was revealed. MGO and GO are highly reactive dicarbonyl compounds that form during glycosylation and precursor structures of CML, one of the most prevalent AGEs in the skin; these compounds are also excellent AGE inducers [25]. Similarly, studies conducted by Guillon [26] et al. showed that carbonyl compounds are excellent cellular models for studying skin complications associated with diabetes. Therefore, in the present study, 4 mM MGO was used for the treatment of skin fibroblasts to simulate the accumulation of AGEs in human skin, and the protective effect of IOP on skin cells in response to this stimulus was examined.

The extract of *I. obliquus* has the potential to be an inhibitor of AGEs [20], but it was unclear which chemical components are the main active ingredients that cause its inhibitory effect. Therefore, in this study, *I. obliquus* extract was further extracted with different polar solvents, and the experimental results showed that the main active components in the different extraction fractions were different. The ethyl acetate fraction contained a higher polyphenol content of approximately 12.85%, the polysaccharide fraction contained a markedly higher polysaccharide content of approximately 29.9%, and the n-hexane fraction contained mainly triterpene components (approximately 33.23%). The antiglycation ability of the different fractions was assessed by establishing an in vitro BSA-glucose model and detecting the fluorescence intensity of the AGEs that formed after incubation with BSA-glucose. The experimental results showed that the antiglycation activity of the polysaccharide fraction was higher than that of the other fractions at different concentrations; thus, the polysaccharide component may be the main active constituent of *I. obliquus* extract that exerts AGE-inhibiting effects. The polysaccharide fraction inhibited the final formation of AGEs by trapping and reducing the production of carbonyl compounds during glycation.

Polysaccharide conformational relationships and activity mechanisms are studied by accurately analyzing the polysaccharide structure, and understanding the physical and chemical properties of polysaccharides used for biological applications is helpful for meeting processing requirements in the food industry. We further purified this polysaccharide fraction to produce the water-soluble polysaccharide, IOP. Based on the molecular characterization and property analysis, the GPC assay showed that the relative molecular weight of IOP was 2.396×10^4 (±6.626%) and that IOP was mainly composed of glucose, galactose, xylose, mannose, and arabinose (29.049:21.705:14.857:9.375:7.709). The FT-IR analysis showed that the structure has O–H and C–H stretching vibrations and contains characteristic peaks of α-glycosidic bonds, indicating typical polysaccharide characteristics. The microstructure revealed by AFM indicates that IOP forms polymers by crosslinking and entangling the sugar chains due to intermolecular forces, and the average roughness of the substance was 0.443. The TGA of the IOP showed that it has good thermal stability.

Cellular behavioral dysfunction can occur due to glycosylation, oxidative stress, or the overexpression of inflammatory factors, which are important causes of impaired dynamic cellular homeostasis, prolonged injury, and poor skin conditions [9,10]. The experimental results showed that IOP could reduce the formation of CML (the most prevalent AGE in the skin), as revealed by good inhibitory effects (up to 47.30%) in the range of 6–24 μg/mL.

Studies [27,28] have shown that AGEs increase the expression level of ROS by activating NADPH oxidase, which causes cells to undergo oxidative stress, the most important mechanism by which the inflammatory response is induced. In addition, this increase in the ROS levels is an important factor in the simultaneous formation of endogenous AGEs and oxidative stress. When an organism is under prolonged oxidative stress, the body's original defense mechanisms are depleted, leading to the overproduction and accumulation of ROS, which eventually results in the production of large amounts of AGEs; thus, a feedback loop is initiated. Therefore, reducing oxidative stress caused by glycosylation and decreasing the overexpression of inflammatory factors are important strategies for inhibiting the formation of AGEs and improving skin cell damage caused by the induction of glycosylation [29,30]. In the present study, IOP significantly alleviated MGO-induced oxidative stress and effectively reduced the secretion of IL-1β, IL-6, and TNF-α, which are inflammatory factors in cells.

In addition, AGEs tend to accumulate in the ECM of the dermis and alter the expression of ECM-related genes in fibroblasts, among which the overexpression of MMP-1, MMP-2 and MMP-9 leads to significant decreases in the expression of fibronectin-1, COL-1 and laminin-5, which are important components of the ECM [31–33]. These proteins are important for the normal behavioral functions (including migration and adhesion) of skin cells, and among these, laminin-5 is a major component of the cellular basement membrane

that stimulates cell adhesion and motility during cell development [34]. Through a series of cascade reactions, fibroblasts eventually undergo behavioral dysfunction, which leads to impaired skin conditions. In the present study, MGO was used to induce the glycosylation of skin fibroblasts (CCC-ESF-1 cells), and the results showed that IOP could reduce cell death after stimulation with different concentrations of MGO. The changes in the expression of MMP1, 2 and 9, FN-1, LM-5, and COL-1 mRNA in cells were measured via qRT−PCR. The experimental results showed that IOP could significantly alleviate the MGO-induced increase in the mRNA expression of MMP1, 2 and 9 and subsequently upregulate the mRNA expression of ECM proteins (FN-1, COL-1 and laminin-5). The results from the cell scratch and adhesion assays showed that IOP effectively restored the migration and adhesion functions of the fibroblasts and improved the MGO-induced dysfunction in the behavior of these cells.

As shown in Fig. 8, the above-described results suggest that IOP can effectively inhibit MGO-induced skin glycosylation reactions and ameliorate glycosylation-induced skin cell damage, such as oxidative stress, inflammation, and behavioral dysfunction, which suggests its potential application as an AGE inhibitor in the field of skin care.

4. Conclusion

IOP, which is mainly composed of glucose, galactose, xylose, mannose and arabinose (29.049:21.705:14.857:9.375:7.709), was obtained by extraction, had a molecular weight of 2.396×10^4 ($\pm 6.626\%$) and was able to effectively block the production of AGEs. In addition, to some extent, IOP effectively reduced the AGE-induced increases in inflammatory factor and ROS levels, further preventing the impairment of cell behavior (decreased migration and reduced cell adhesion) and the downregulation of key ECM proteins induced by AGEs. The results indicate the potential application of IOP as an AGE inhibitor for skin care applications.

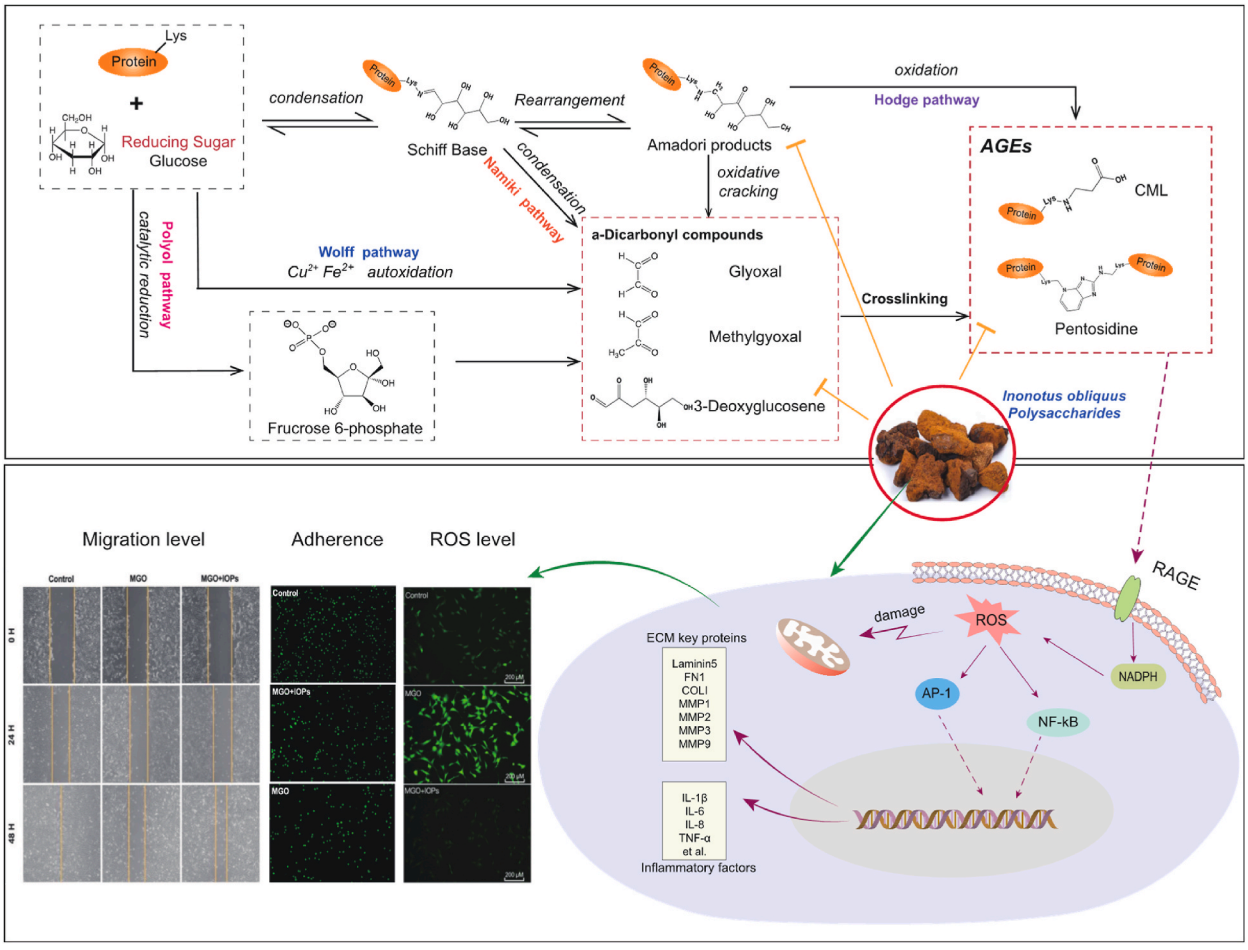

Fig. 8. Mechanisms of the blockade of AGE production and cellular physiological regulation by IOP.

5. Materials and methods

5.1. Materials

I. *obliquus* was purchased from Anguo City, Hebei Province. Human embryonic skin fibroblasts (CCC-ESF-1 cells) were purchased from Peking Union Medical College Hospital. MGO was purchased from Merck & Co., Inc. DMEM, fetal bovine serum, penicillin–streptomycin, and 0.25% trypsin (including EDTA) were purchased from Thermo Fisher Scientific Co., Ltd. (China). Cell Counting Kit-8, Western and IP cell lysis buffer and PMSF were purchased from Beyotime Biotechnology Co., Ltd. TRIzol was purchased from Suolgaibao Biological Technology Co., Ltd.

5.2. Extraction and analysis of the active ingredients of I. obliquus

I. *obliquus* 75% ethanol extract was mixed at a material–liquid ratio of 1:10, and the extract was sonicated for 120 min at 40 °C, 560 W and 40 kHz in an ultrasonicator. After filtration, the filtrate and filtrate residue were collected separately and used in the next step of the experiment.

The filtrate was concentrated to a volume of 50 mL under vacuum at 40 °C. The hexane, ethyl acetate, n-butanol and concentrated filtrates were mixed well at a ratio of 1:1 each, and the extracts were then allowed to separate for 1 h. The different parts of the extracts were collected to obtain the n-hexane, ethyl acetate and n-butanol extracts.

The filtrate was mixed with water at a ratio of 1:20 and refluxed at 100 °C for 3 h. The filtrate was then filtered to obtain a new filtrate. The newly collected filtrate was concentrated under vacuum and reduced pressure to an appropriate volume, mixed with 3 times the volume of anhydrous ethanol and allowed to stand overnight at 4 °C. The precipitate was then collected by centrifugation. The precipitate was then collected by centrifugation to obtain the crude polysaccharide (IOPsc).

The four solutions obtained as described above were freeze-dried to obtain the target extracts. The polysaccharide, total polyphenol and total triterpene contents of the extracted fractions (n-hexane, ethyl acetate, n-butanol and polysaccharide) were determined by the phenol–sulfuric acid, Folin–Ciocalteu and vanillin–glacial acetic acid–perchloric acid colorimetric methods, respectively.

5.3. Detection of the inhibitory ability of glycation end products

The bovine serum albumin (BSA)-fructose reaction solution was prepared according to the methods described by Spagnuolo L et al. [35]. The four extracted fractions were diluted to five different concentrations (1000, 500, 250, 125 and 62.5 μg/mL) with PBS (pH 7.3, containing 0.02% sodium azide). The BSA-fructose reaction solution was then mixed with equal volumes of each sample solution. PBS (pH 7.3, containing 0.02% sodium azide) and an equal volume of sample solution were used as blank controls, aminoguanidine was used as a positive control, and PBS (pH 7.3, containing 0.02% sodium azide) was used as a negative control. Each sample was incubated in a constant-temperature incubator at 37 °C for 5 days while protected from light.

Determination of the glycated serum protein (GSP) content: This experiment was performed according to the methods described by Liu et al. with modifications [36]. Glycosylated BSA (10 mL) was mixed with 200 mL of nitro blue tetrazolium (NBT) chromogenic solution in the sample wells. Additionally, 10 mL of BSA was mixed with 2 mmol/L N,N-dimethylformamide (DMF) in the standard wells. The samples were incubated for 3 days, and the OD at 530 nm was then measured at 37 °C for 15 min.

$$C_{GSP}(mM) = \frac{OD_{sp} - OD_{sp\ control}}{OD_{sd} - OD_{sd\ control}} \times C_{sd}(2\ mM)$$

Determination of reactive carbonyl compounds: The nonenzymatic glycation system was incubated for 4 days. A total of 0.125 mL of sample solution was mixed with 0.750 mL of double-distilled water, 0.125 mL of 2,4-dinitrophenylhydrazine (DNPH) solution was added, and the absorbance was measured at 370 nm for 5 min.

$$C_{Carbonyl\ compound}\left(\frac{mg}{mL}\right) = \frac{OD_{sp} - OD_{sp\ control}}{OD_{sd} - OD_{sp\ control}} \times \text{sample dilution}$$

Determination of AGEs: The nonenzymatic glycation system was incubated for 5 days, and the fluorescence at an excitation wavelength of 370 nm and an emission wavelength of 440 nm was then measured via fluorescence zymography. The inhibition rate (IR) of the AGEs was calculated as follows:

$$IR\ (\%) = \left(1 - \frac{RFU_{Inhibition} - RFU_{Control}}{RFU_{negative\ control}}\right) \times 100\%$$

5.4. UV–Vis

The polysaccharide solution obtained as described above was treated by the Savage method. The organic reagents and excess small molecule impurities were then dialyzed using dialysis bags, and the pigments present in the solution were adsorbed by AB-8 macroporous adsorbent resin. Using the phenol–sulfuric acid method for septal tube tracking detection, the number of elution tubes was used as the horizontal coordinate, and the absorbance of the polysaccharide eluent was used as the vertical coordinate; the elution

curve was used to merge the eluents of the same components, which were concentrated and freeze-dried to obtain the different components of the purified polysaccharide from Birch fucoidan IOP.

The absorbance of IOP in the range of 200–800 nm was measured using a UV–visible spectrophotometer to detect the presence of distinct nucleic acid and protein absorption peaks.

5.5. FT-IR

The molecular structures of the IOP were analyzed with a Nicolet™ iSTM10 (Thermo Fisher Scientific, USA) in the wavelength range of 500–4000 cm^{-1} at a resolution of 1 cm^{-1}.

5.6. Monosaccharide composition analyses

IOP and standards were hydrolyzed and derivatized according to the methods described by Su et al. [37]. The signal at 250 nm was detected using an LC-20AD instrument (Shimadzu, Japan) equipped with an Xtimate C18 column (4.6*200 mm, 5 μm) after elution at a flow rate of 1 mL/min at 30 °C. The mobile phase was 0.05 M potassium dihydrogen phosphate solution (pH 6.70, adjusted with sodium hydroxide):acetonitrile at a ratio of 83:17.

5.7. GPC

The molecular weight distribution of IOP was determined by gel permeation chromatography with an eighteen-angle laser light scattering instrument and a differential refractive index detector (GPC-LS-RI).

5.8. AFM

AFM imaging was performed using a Dimension Icon three-directional closed loop scanner (Bruker AXS, Germany) in the scan range of 90 μm*90 μm in the XY direction with overall noise below the 0.03-nm RMS value.

5.9. TGA

A simultaneous thermal analyzer (Netzsch, Germany) was used to analyze the relationship between the physical or chemical parameters of IOP and the temperature. Thermogravimetric Analysis (TGA) and differential scanning calorimetry (DSC) were performed as the temperature was increased from room temperature to 800 °C at a rate of 10 K/min under a nitrogen atmosphere.

5.10. Cell proliferation assay

A CCC-ESF-1-cell suspension was added to 96-well plates at 10,000 cells per well and incubated in a cell incubator for 12 h. The medium was changed to basal medium containing IOP and different concentrations of MGO for an additional 24 h of incubation. The medium was then discarded, and 100 μL of basal medium containing 10% CCK8 was added to each well for 2 h of incubation. The absorbance at 450 nm was measured using an enzyme reader.

5.11. ROS detection

CCC-ESF-1 cells were incubated in a 6-well plate, 2 mL of DCFH-DA was added to each well according to the instructions of the Reactive Oxygen Species Assay Kit (S0033S, Beyotime), and the plate was incubated in the incubator for 25 min in the dark. The six-well plates were removed from the incubator and washed 3 times with PBS. Then, 1 mL of PBS was added to each well, and the wells were photographed under an inverted fluorescence microscope. The cells in each well were then removed by scraping with a cell spatula, 200 μL of the contents of each well was transferred to a black 96-well plate, and the fluorescence signals obtained with an excitation wavelength of 488 nm and an emission wavelength of 525 nm were detected by a fluorescence enzyme reader.

5.12. ELISAs for assessing carboxymethyl lysine (CML) and inflammatory factors

We added a cell suspension to 6-well plates at 400,000 cells per well for incubation with complete medium. After the cells had grown to 70–80% confluence, the medium was replaced with basal medium containing 4 mM MGO (model group), basal medium (blank group), or basal medium containing 4 mM MGO and different concentrations of IOP (sample groups), and the cells were incubated for 2 days. At the end of the incubation, 200 μL of Western and IP cell lysis solution (containing 1% PMSF) was added to each well to lyse the cells for 2 min, the lysate was collected and centrifuged at 10000 rpm at 4 °C for 5 min, and the supernatant was carefully collected. The levels of CML and inflammatory factors in the collected cell lysates were determined using a Human Carboxymethyl Lysine (CML) ELISA Kit (CUSABIO, https://www.cusabio.com/) and a Human IL-1β/IL-6/TNF-α ELISA Kit (Beyotime, https://www.solarbio.com/), respectively.

5.13. Cell migration rate and adhesion test

Cell adhesion was measured using a Cell Adhesion Assay Kit (BB-48123, Bestbio). First, 100 μL of coating solution was added to each well of a 96-well plate, and the plate was incubated overnight at 4 °C. After removing the coating solution, the 96-well plate was dried and washed three times with washing solution. The cells were incubated with the sample for 1 h. The medium was discarded, and 200 μL of basal medium and 10 μL of BBcell Probe C07 fluorescence staining solution were added to each well for the observation and assessment of cell adhesion via an inverted fluorescence microscope and a fluorescence enzyme reader, respectively, at an excitation wavelength of 488 nm and an emission wavelength of 520 nm.

CCC-ESF-1 cells were incubated in 6-well plates until reaching 80% confluence, and three parallel linear scratches were made in each well before stimulation and incubation with MGO and IOP. The degree of cell scratch healing was observed at 24 h and 48 h.

$$\text{Scratch area recovery rate}(\%) = \frac{\text{0h Scratch area} - \text{24/48h Scratch area}}{\text{0h Scratch area}}$$

5.14. qRT–PCR

After the CCC-ESF-1 cells were incubated in a 6-well plate, 1 mL of TRIzol was added to each well for 2 min of reaction. The cells were then transferred to a 1.5-mL EP tube, 200 μL of chloroform was added, and the tubes were shaken vigorously. After standing for 5 min, the tubes were centrifuged at 12000 rpm for 15 min at 4 °C. The upper layer of solution was mixed with an equal volume of isopropanol, left for 10 min, and then centrifuged at 12,000 rpm for 15 min at 4 °C. The supernatant was carefully discarded, 1 mL of 75% ethanol (prechilled at −20 °C) was added, and the samples were allowed to stand for 5 min and then centrifuged at 12000 rpm for 5 min at 4 °C. The supernatant was carefully aspirated, the cap was opened to allow the ethanol to evaporate, and 30 μL of DNase-free water was added.

The UEIris II RT–PCR System for First-Strand cDNA Synthesis (BN12028, Biorigin (Beijing) Inc.) was used for reverse transcription. Fast Super EvaGreen® qPCR Master Mix (BN12008, Biorigin (Beijing) Inc.) was used for the qPCR assays. The primers used in this study were all designed in the NCBI (https://www.ncbi.nlm.nih.gov/) platform and are shown in Table 1.

5.15. Statistical analysis

The data in this paper are supported by three or more parallel experiments and are expressed as the means ± standard deviations. Data visualization and statistical analysis were performed using GraphPad Prism 9 and ImageJ. Statistical analyses were performed by one-way and two-way ANOVA to identify significant differences.

Funding

This work was supported by the Scientific Research Project of the Beijing Educational Committee (KM202010011009) and the Beijing Excellent Talent Training Project-Young Individuals (2018000020124G032), both of which provided funding support to Pr. Fan YI.

Ethics approval and consent to participate

Not applicable.

Data availability statement

The authors declare that the data supporting the findings of this study are available within the paper, a request for more detailed data should be sent to the corresponding authors with the permission of all authors.

Additional information

No additional information is available for this paper.

CRediT authorship contribution statement

Chunyu Chen: Writing – original draft. **Xiaoxing Liu:** Data curation. **Yingying Lin:** Visualization. **Li Li:** Resources, Project administration. **Miaomiao Guo:** Resources, Methodology, Conceptualization. **Fan Yi:** Writing – review & editing, Funding acquisition, Conceptualization.

Declaration of competing interest

The authors declare that they have no known competing financial interests or personal relationships that could have appeared to

Table 1
Primer sequences.

Primer	Primer sequence
β-Actin-F	CGCGAGAAGATGACCCAGAT
β-Actin-R	GCACTGTGTTGGCGTACAGG
Laminin-5-F	GGACTGCAGGCCACCG
Laminin-5-R	AGGATGCCCACAAACTCCAG
COLI-F	AGTGGTTTGGATGGTGCCAA
COLI-R	GCACCATCATTTCCACGAGC
FN1–F	TCAGCTTCCTGGCACTTCTG
FN1-R	TCTTGTCCTACATTCGGCGG
MMP-1-F	TGTGGTGTCTCACAGCTTCC
MMP-1-R	CGCTTTTCAACTTGCCTCCC
MMP-2-F	GTCTGTGTTGTCCAGAGGCA
MMP-2-R	CTAGGCCAGCTGGTTGGTTC
MMP-9-F	TCAGCTTCCTGGCACTTCTG
MMP-9-R	TCTTGTCCTACATTCGGCGG

influence the work reported in this paper.

Acknowledgments

We thank Yongtao Zhang for the helpful discussions and the assistance provided with this work.

References

[1] Q. Jin, R.C.W. Ma, Metabolomics in diabetes and diabetic complications: insights from epidemiological studies, Cells 10 (11) (2021).
[2] E. Makrantonaki, D. Jiang, A.M. Hossini, G. Nikolakis, M. Wlaschek, K. Scharffetter-Kochanek, C.C. Zouboulis, Diabetes mellitus and the skin, Rev. Endocr. Metab. Disord. 17 (3) (2016) 269–282.
[3] G.M. de Macedo, S. Nunes, T. Barreto, Skin disorders in diabetes mellitus: an epidemiology and physiopathology review, Diabetol. Metab. Syndrome 8 (1) (2016) 63.
[4] J. Salazar, C. Navarro, Á. Ortega, M. Nava, D. Morillo, W. Torres, M. Hernández, M. Cabrera, L. Angarita, R. Ortiz, M. Chacín, L. D'Marco, V. Bermúdez, Advanced glycation end products: new clinical and molecular perspectives, Int. J. Environ. Res. Publ. Health 18 (14) (2021).
[5] M.T. Goova, J. Li, T. Kislinger, W. Qu, Y. Lu, L.G. Bucciarelli, S. Nowygrod, B.M. Wolf, X. Caliste, S.F. Yan, D.M. Stern, A.M. Schmidt, Blockade of receptor for advanced glycation end-products restores effective wound healing in diabetic mice, Am. J. Pathol. 159 (2) (2001) 513–525.
[6] S.L. Fan, J.A. Lin, S.Y. Chen, J.H. Lin, H.T. Lin, Y.Y. Chen, G.C. Yen, Effects of Hsian-tsao (Mesona procumbens Hemsl.) extracts and its polysaccharides on the promotion of wound healing under diabetes-like conditions, Food Funct. 12 (1) (2021) 119–132.
[7] H. Liao, J. Zakhaleva, W. Chen, Cells and tissue interactions with glycated collagen and their relevance to delayed diabetic wound healing, Biomaterials 30 (9) (2009) 1689–1696.
[8] C. Qing, The molecular biology in wound healing & non-healing wound, Chin. J. Traumatol. 20 (4) (2017) 189–193.
[9] H. Liao, I. Pastar, W. Chen, Rosiglitazone modulates the behaviors of diabetic host-derived fibroblasts in a carboxymethyllysine-modified collagen model, Wound Repair Regen. 20 (3) (2012) 435–443.
[10] D.M. Bermudez, B.J. Herdrich, J. Xu, R. Lind, D.P. Beason, M.E. Mitchell, L.J. Soslowsky, K.W. Liechty, Impaired biomechanical properties of diabetic skin implications in pathogenesis of diabetic wound complications, Am. J. Pathol. 178 (5) (2011) 2215–2223.
[11] V.P. Reddy, Oxidative stress in health and disease, Biomedicines 11 (11) (2023).
[12] K.C. Sourris, A. Watson, K. Jandeleit-Dahm, Inhibitors of advanced glycation end product (AGE) formation and accumulation, Handb. Exp. Pharmacol. 264 (2021) 395–423.
[13] S. Khangholi, F.A. Majid, N.J. Berwary, F. Ahmad, R.B. Aziz, The mechanisms of inhibition of advanced glycation end products formation through polyphenols in hyperglycemic condition, Planta Med. 82 (1–2) (2016) 32–45.
[14] C.R. Sruthi, K.G. Raghu, Methylglyoxal induces ambience for cancer promotion in HepG2 cells via Warburg effect and promotes glycation, J. Cell. Biochem. 123 (10) (2022) 1532–1543.
[15] Y. Zhang, H. Ma, W. Liu, T. Yuan, N.P. Seeram, New antiglycative compounds from cumin (cuminum cyminum) spice, J. Agric. Food Chem. 63 (46) (2015) 10097–10102.
[16] J. Monte-Serrano, P. Villagrasa-Boli, J. Cruañes-Monferrer, P. Arbués-Espinosa, S. Martínez-Cisneros, M.F. García-Gil, [The role of metformin in the treatment of dermatological diseases: a narrative review], Atención Primaria 54 (6) (2022) 102354.
[17] V. M, K. Wang, Dietary natural products as a potential inhibitor towards advanced glycation end products and hyperglycemic complications: a phytotherapy approaches, Biomed. Pharmacother. 144 (2021) 112336.
[18] K.A. Szychowski, B. Skora, T. Pomianek, J. Gminski, Inonotus obliquus - from folk medicine to clinical use, J Tradit Complement Med 11 (4) (2021) 293–302.
[19] Y. Zhao, W. Zheng, Deciphering the antitumoral potential of the bioactive metabolites from medicinal mushroom Inonotus obliquus, J. Ethnopharmacol. 265 (2021) 113321.
[20] C. Wang, X. Gao, R.K. Santhanam, Z. Chen, Y. Chen, L. Xu, C. Wang, N. Ferri, H. Chen, Effects of polysaccharides from Inonotus obliquus and its chromium (III) complex on advanced glycation end-products formation, alpha-amylase, alpha-glucosidase activity and H2O2-induced oxidative damage in hepatic L02cells, Food Chem. Toxicol. 116 (Pt B) (2018) 335–345.
[21] J. Wang, W. Hu, L. Li, X. Huang, Y. Liu, D. Wang, L. Teng, Antidiabetic activities of polysaccharides separated from Inonotus obliquus via the modulation of oxidative stress in mice with streptozotocin-induced diabetes, PLoS One 12 (6) (2017) e0180476.
[22] Q. Wu, M. Luo, X. Yao, L. Yu, Purification, structural characterization, and antioxidant activity of the COP-W1 polysaccharide from Codonopsis tangshen Oliv, Carbohydr. Polym. 236 (2020) 116020.
[23] X. Zhang, Z. Liu, C. Zhong, Y. Pu, Z. Yang, Y. Bao, Structure characteristics and immunomodulatory activities of a polysaccharide RGRP-1b from radix ginseng Rubra, Int. J. Biol. Macromol. 189 (2021) 980–992.
[24] Y. Chen, Y. Xue, Purification, chemical characterization and antioxidant activities of a novel polysaccharide from Auricularia polytricha, Int. J. Biol. Macromol. 120 (Pt A) (2018) 1087–1092.
[25] C.Y. Chen, J.Q. Zhang, L. Li, M.M. Guo, Y.F. He, Y.M. Dong, H. Meng, F. Yi, Advanced glycation end products in the skin: molecular mechanisms, methods of measurement, and inhibitory pathways, Front. Med. 9 (2022) 837222.

[26] C. Guillon, S. Ferraro, S. Clement, M. Bouschbacher, D. Sigaudo-Roussel, C. Bonod, Glycation by glyoxal leads to profound changes in the behavior of dermal fibroblasts, BMJ Open Diabetes Res Care 9 (1) (2021).
[27] B.I. Hudson, M.E. Lippman, Targeting RAGE signaling in inflammatory disease, Annu. Rev. Med. 69 (2018) 349–364.
[28] A. Bierhaus, P.M. Humpert, M. Morcos, T. Wendt, T. Chavakis, B. Arnold, D.M. Stern, P.P. Nawroth, Understanding RAGE, the receptor for advanced glycation end products, J. Mol. Med. (Berl.) 83 (11) (2005) 876–886.
[29] S. Shin, D. Son, M. Kim, S. Lee, K.-B. Roh, D. Ryu, J. Lee, E. Jung, D. Park, Ameliorating effect of akebia quinata fruit extracts on skin aging induced by advanced glycation end products, Nutrients 7 (11) (2015) 9337–9352.
[30] F.J. Hidalgo, R. Zamora, Interplay between the maillard reaction and lipid peroxidation in biochemical systems, Ann. N. Y. Acad. Sci. 1043 (2005) 319–326.
[31] H. Pageon, H. Zucchi, F. Rousset, V.M. Monnier, D. Asselineau, Skin aging by glycation: lessons from the reconstructed skin model, Clin. Chem. Lab. Med. 52 (1) (2014) 169–174.
[32] K.H. Lee, Y.P. Ng, P.S. Cheah, C.K. Lim, M.S. Toh, Molecular characterization of glycation-associated skin ageing: an alternative skin model to study in vitro antiglycation activity of topical cosmeceutical and pharmaceutical formulations, Br. J. Dermatol. 176 (1) (2017) 159–167.
[33] C. Lohwasser, D. Neureiter, B. Weigle, T. Kirchner, D. Schuppan, The receptor for advanced glycation end products is highly expressed in the skin and upregulated by advanced glycation end products and tumor necrosis factor-alpha, J. Invest. Dermatol. 126 (2) (2006) 291–299.
[34] B.P. Nguyen, M.C. Ryan, S.G. Gil, W.G. Carter, Deposition of laminin 5 in epidermal wounds regulates integrin signaling and adhesion, Curr. Opin. Cell Biol. 12 (5) (2000) 554–562.
[35] L. Spagnuolo, S. Della Posta, C. Fanali, L. Dugo, L. De Gara, Antioxidant and antiglycation effects of polyphenol compounds extracted from hazelnut skin on advanced glycation end-products (AGEs) formation, Antioxidants 10 (3) (2021).
[36] H. Liu, C. Wang, X. Qi, J. Zou, Z. Sun, Antiglycation and antioxidant activities of mogroside extract from (Swingle) fruits, J. Food Sci. Technol. 55 (5) (2018) 1880–1888.
[37] Y. Su, Y. Zhang, H. Fu, F. Yao, P. Liu, Q. Mo, D. Wang, D. Zhao, C. Wang, M. Li, Physicochemical and anti-UVB-induced skin inflammatory properties of lacticaseibacillus paracasei subsp. paracasei SS-01 strain exopolysaccharide, Fermentation 8 (5) (2022) 198.